New Insights into the Reaction Mechanisms of Phenylium Ions with Benzene†

Daniela Ascenzi,* Nives Cont, Graziano Guella, Pietro Franceschi,‡ and Paolo Tosi

Dipartimento di Fisica, Università di Trento, Via Sommarive 14, 38050 Povo (TN), Italy

Received: July 25, 2007; In Final Form: August 30, 2007

The chemistry of phenylium (benzen-1-ylium) cations with benzene is investigated by using a guided ion beam tandem mass spectrometer. The main ionic products from the reaction of $C_6H_5^+$ with C_6H_6 are observed at *m*/*z* 155 (covalent adduct $C_{12}H_{11}^+$), 154 ($C_{12}H_{10}^+$), 153 ($C_{12}H_9^+$), 129 ($C_{10}H_9^+$), and 115 ($C_9H_7^+$). We propose a mechanism according to which channels at *m*/*z* 154−115 are formed by elimination of stable neutral molecules (such as H_2, C_2H_2, C_3H_4) from the collision complex $C_{12}H_{11}^+$, for which the most plausible structure is protonated biphenyl. The proposed mechanism is demonstrated by using partial isotopical labeling of reagents to look for possible H/D atom scrambling. Almost the same ions are produced when benzene is chemically ionized at atmospheric pressure in an APCI source from which oxygen is excluded. Because an ion trap analyzer is coupled to this source, tandem MS experiments can be performed, allowing structural details to be established. Moreover, the use of partially deuterated reagents has allowed the detection of minor reactive channels resulting from charge exchange and H^-/D^- hydride-transfer processes. Theoretical calculations show that the most stable structure for ions at *m*/*z* 129 $C_{10}H_9^+$ is that of protonated naphthalene, resulting from the loss of an acetylene molecule by the condensation product, with a reaction exothermicity of 1.27 eV. We have found a possible barrierless pathway for such a channel that might be viable for the synthesis of naphthalene, the smallest PAH, even at low collision energies and therefore would be of particular astrochemical relevance.

1. Introduction

The phenylium cation/benzene system is important for the synthesis of polyaromatic hydrocarbons (PAHs), occurring either in combustion processes or in interstellar clouds. Alongside the well-established radical mechanisms developed to explain the growth of PAHs, such as the HACA mechanism,[1] recently an alternate ionic route has been proposed for the synthesis of PAHs under the cold and dilute conditions of interstellar matter. Such a mechanism proceeds through a series of condensation reactions of hydrocarbon dications $C_mH_n^{2+}$ ($m = 6-10$, $n = 4-9$) with neutral benzene.[2,3] It cannot be ignored, however, that the production of polymeric aggregates might derive from reactions of singly charged ions on benzene itself through the well-known mechanism of electrophilic aromatic substitution.

In a previous paper[4] we have shown that, in the presence of oxygen, plasma treatment of benzene leads mainly to the production of phenol and heavier O-containing species. When oxygen is removed, leaving a mixture of benzene and N_2, the main molecular products after plasma treatment are biphenyl compounds.[5] The principal motivation for the present study is understanding the chemical steps leading to biphenyl synthesis in benzene plasmas operating at atmospheric pressure in the absence of oxidizing species.

The synthesis of diaryl molecules is of paramount importance in organic chemistry and a major effort is currently dedicated to understanding possible mechanisms for coupling of aromatic compounds.[6,7] The aryl−aryl bond formation represents a key step in modern organic synthesis,[8] and it is mostly accomplished through a reductive symmetrical coupling of aryl halides (Ullmann reaction) or via cross-coupling reactions between aryl halides and organometallic reagents. The production of biphenyl from benzene in an atmospheric pressure plasma relies instead on the catalytic role of the plasma, which oxidizes C_6H_6 to $C_6H_5^+$ and initiates the direct arylation process.

Biphenyl, as well as other C_{12} compounds, is the main hydrocarbon product observed in the radiolysis of liquid[9] and gaseous benzene.[10,11] There has been a long standing argument on the mechanisms responsible for the production of biphenyl under such "high density'' conditions. One possible mechanism involves the participation of free radicals such as $C_6H_5^\bullet$ and benzene molecules in electronically excited states, but some experimental evidence suggests that biphenyl formation is due, at least partially, to ion−molecule reactions.[9,11,12] We believe this could be the case even under our high-pressure plasma conditions.

According to the radical mechanism, the excited benzene formed by radiation (or in a plasma) initially decomposes to a phenyl radical plus a hydrogen atom. Subsequently, one possible route to biphenyl is the recombination of two phenyl radicals:

$$C_6H_5^\bullet + C_6H_5^\bullet \rightarrow C_{12}H_{10} \qquad (1)$$

The rate constant for process 1 is 1.92×10^{-11} cm^3 s^{-1} at 300 K.[13] Despite the high value of the rate constant, the overall production of biphenyl via such a process is certainly limited by the low probability of a radical−radical encounter in an environment in which the density of radicals is low compared to neutrals.

Alternatively, the formation of biphenyl may take place by the following addition−elimination process

† Part of the "Giacinto Scoles Festschrift".

* Corresponding author. Phone:+39 0461 881693. Fax:+39 0461 881696. E-mail: ascenzi@science.unitn.it.

‡ Present address: Sincrotrone Trieste, AREA Science Park, Basovizza, Trieste, Italy.

10.1021/jp075860h CCC: $37.00
Published on Web 11/02/2007

$$C_6H_5^{\bullet} + C_6H_6 \rightarrow C_{12}H_{11} \rightarrow C_{12}H_1 + H \quad (2)$$

but the overall rate constant for such a process is very small (8.14×10^{-16} cm^3 s^{-1} at 300 K[14,15]) and therefore it is not likely to play a role.

An ionic mechanism has been proposed,[12] which starts with the ionization of benzene to give $C_6H_6^+$ and comprises the following steps:

$$C_6H_6^+ + C_6H_6 \xrightarrow{k_3} C_{12}H_{12}^+ \quad (3)$$

$$C_{12}H_{12}^+ + e^- \rightarrow C_{12}H_{10} + H_2 \quad (4)$$

However, the rate constant for the formation of a benzene dimer complex according to eq 3 is rather small. A value for k_3 of about 7×10^{-12} cm^3 s^{-1} was measured at thermal energies,[16] but the observation of this species usually requires collisional stabilization[17−20] and $C_{12}H_{12}^+$ was not detected in experiments performed in low-pressure environments (10^{-5}−10^{-4} mbar).[21]

An alternate ionic route to biphenyl synthesis is the reaction of phenyl cation, which is known to be formed upon electron impact ionization of benzene:

$$C_6H_5^+ + C_6H_6 \xrightarrow{k5a} C_{12}H_{11} + \xrightarrow{k5b} C_{12}H_{10}^{+\bullet} + H^{\bullet} \quad (5)$$

Once biphenyl is formed as an ion, it can be neutralized easily by collisions with electrons or with the reactor's wall. The first step of the ionic mechanism is the association of a phenylium ion with a benzene molecule to give the condensation product $C_{12}H_{11}^+$ and the rate constant k_{5a} for such a process at thermal energy has been measured to be (3−4.3) $\times 10^{-10}$ cm^3 s^{-1},[16] 8.6×10^{-11} cm^3 s^{-1},[21] and 1.17×10^{-10} cm^3 s^{-1}.[22] The second step is an H atom elimination from the condensation products: a direct measurement of its rate constant has not been performed; however, a value of 5.4×10^{-11} cm^3 s^{-1} for the overall process (5) can be inferred from the total rate coefficient and branching ratio of the reaction of phenylium cation with benzene.[21] Due to the higher value of the rate constant compared to the radical reactions, we believe that process 5 is the pathway leading to biphenyl formation in benzene plasma systems.

It has been proposed[11,22] that, upon electron impact ionization of benzene vapors at low pressure (4×10^{-4} mbar), the biphenyl cation can be formed also via reaction of $C_6H_4^+$ ions with benzene:

$$C_6H_4^+ + C_6H_6 \rightarrow C_{12}H_{10}^{+\bullet} \quad (6)$$

We have investigated the reactivity of $C_6H_4^+$ with benzene in our apparatus, and we found that the main product is due to electron transfer from benzene to give $C_6H_6^{+\bullet}$. Therefore we believe reaction 6 is not relevant for biphenyl formation in benzene plasma systems.

Secondary reactions between benzene and its fragment ions, among which is $C_6H_5^+$, obtained by electron bombardment of benzene in sources at pressures where multiple collisions are possible (10^{-4}−10^{-3} mbar) have been investigated by mass spectrometric techniques.[11,16,22]

The bimolecular reaction of $C_6H_5^+$ with benzene has been studied at thermal energies and under low-pressure conditions (10^{-6}−10^{-5} mbar) by tandem ICR mass spectrometry[20] and trapped ion mass spectrometry.[21] A comparison between present and previous results on the reactivity of phenylium cation with benzene is discussed in section 4.

2. Experimental Methods

Reactions have been studied by using a guided-ion-beam tandem mass spectrometer (GIB-MS) that has been described previously, along with the data analysis procedure.[23,24] Recently, the apparatus has been upgraded by adding a further octopole ion guide after the ion source and a description of the setup is given in the following. Ions are generated in an electron impact source (at variable electron energies, usually in the range 30−40 eV), and they are extracted by a set of conical extractor lenses, to be injected into a first octopole (length 8.2 cm, radius 0.9 cm). Phenylium cations and their deuterated analogues are produced in high yields by electron impact dissociative ionization of C_6H_5Cl (Sigma-Aldrich, 99.8% purity) or C_6D_5Br (Sigma-Aldrich, purity > 99.5% D atoms). The octopole is surrounded by a cell that can be filled with an inert gas (usually He is employed) via a variable leak valve. In this way reagent ions can quench their internal energy by collisions with the inert gas into the first octopole. To check the effect of collisional relaxation of He on the ions emerging from the source, we have measured the amount of unimolecular fragmentation of excited $C_6H_5^{+}$* ions into $C_4H_3^+$ (m/z 51)$^+$ and C_2H_2 during their flight from the source into the detector (the flight time into our setup is about 10^{-4} −10^{-3} s). When He is added into the first octopole, we observe a decrease of the fragmentation yield by a factor of ≈5, i.e., from 0.5% to 0.1%.

After the cooling stage, an Einzel lens transports the ions into a first mass spectrometer, which is used to mass-select the primary ion beam. The chosen reactant ions are injected into the second octopole ion guide (length 10.2 cm, radius 0.6 cm) by a six-element accelerating/decelerating cylindrical lens whose last element has a conical shape to limit the angular divergence of the ion beam entering the octopole to 41°. The second octopole is surrounded by the scattering cell, where mass-selected ions react with neutral C_6H_6 (Fluka, UV spectroscopy grade) or C_6D_6 (Fluka, purity >99.5% D atoms). Benzene vapors are introduced in the scattering cell through a leak valve, with the pressure generally set near 5×10^{-5} mbar (as measured by a spinning rotor gauge MKS SRG2) to ensure single collision conditions. The ion beam kinetic energy can be varied by changing the second octopole dc potential with respect to the ion source. Product ions and unreacted primary ions are collected by the octopole ion guide, mass analyzed by a second quadrupole and, after a 90° deflection, detected by an electron multiplier.

The ratio between the measured signal intensities of product and reactant ions is proportional to the effective integral reactive cross section σ_{eff} and its absolute value can be measured, in a beam-cell experiment, according to the Lambert−Beer law:

$$\frac{I_P}{I_0} = \sigma_{eff} n l_{eff} \quad (7)$$

where I_P and I_0 are the intensities of products P and reagent ions respectively (with $I_P \ll I_0$), n is the gas density in the scattering cell, and l_{eff} is the effective length of the collision cell, which may differ from the length of the octopole due to conductance effects at the edges of the octopole. By measuring the slope of the plot of I_P/I_0 as a function of benzene gas density (at low gas densities to ensure single collision regime), we can derive σ_{eff} if l_{eff} is known. The effective length l_{eff} of our setup was measured using the test case reaction $Ar^+ + H_2 \rightarrow ArH^+$,

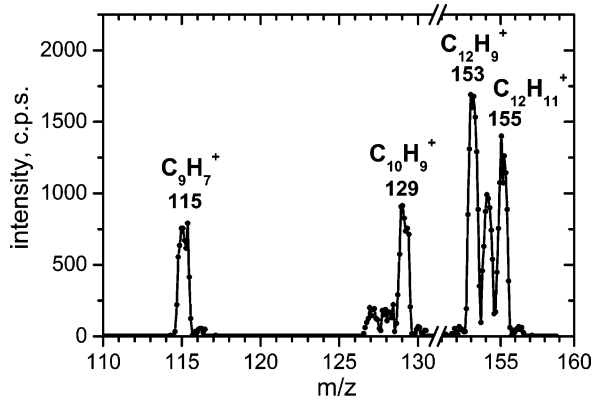

Figure 1. Mass spectrum of product ions resulting form the reaction of $C_6H_5^+$ with C_6H_6 in the GIB-MS setup. The collision energy is E_{cm} = 0.46 eV and benzene pressure in the reaction cell is 5×10^{-5} mbar.

for which the integral cross section is known.[25] A value of $l_{eff} = 12.0 \pm 0.6$ cm is obtained. The accuracy of our data is limited by the measurement of the gas pressure within the scattering cell and by error propagation due to the calibration procedure. We estimate that our absolute cross-section values are accurate within ±30%.

APCI-MS experiments were performed in a Bruker Esquire-LC quadrupole ion-trap mass spectrometer equipped with an APCI interface (HP/Agilent Technologies). Details of the experimental apparatus have been described previously.[5] High purity N_2 used as nebulizer and dry gas (with a flow of 6 l/min at a temperature of 300 °C) was obtained from the boil-off of a liquid nitrogen dewar. The temperature of the source region was typically kept at 450 °C during measurements. A 1:1 mixture of benzene and deuterated benzene was introduced as liquid by a micrometric syringe pump at a flow rate of 0.1 mL/min. The mass spectrometer is operated with a scan rate of 13 000 u/s, and mass spectra were collected in the full scan mode are obtained by scanning over the range *m*/*z* 15−300. MS/MS experiments have been carried out by resonant activation of the precursor ions by using He gas in the trap. To avoid contamination from back-streaming O_2, the gas pressure in the source has been kept slightly higher than the atmospheric one. The absence of oxygen in the discharge region is proven by the absence of oxygen containing species in comparison with the spectra presented in our previous study.[4]

3. Theoretical Methods

Ab initio quantum chemical calculations have been performed with the B3LYP hybrid exchange-correlation functional and MP2 methods implemented in Spartan 04 (Wavefunction Inc., Irvine, CA). Structure optimizations were carried out using the density functional method at the B3LYP/6-31G* level of theory, and energies of the most relevant stationary points (intermediate adducts and transition states) were calculated at the MP2/6-311++G** level.

4. Results and Discussion

We have studied the reaction of phenylium cations with benzene, by using also isotopically labeled reagents. The $C_6H_5^+ + C_6D_6$ and $C_6D_5^+ + C_6H_6$ isotope combinations were used to look for possible atom scrambling during the reaction and to observe channels leading to back-fragmentation of the adduct into reactants. When using hydrogenated reagents $C_6H_5^+ + C_6H_6$ product ions appear mainly at *m*/*z* 155, 154, 153, 129, and 115 and a mass spectrum of products is shown in Figure 1.

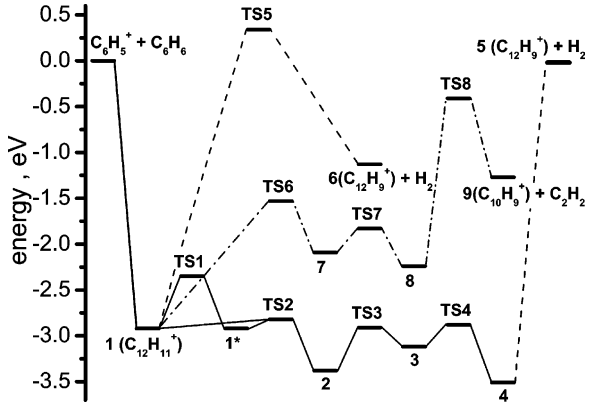

Figure 2. Schematic representation of the $C_6H_5^+ + C_6H_6$ potential energy profile. Energies are derived from calculations at the MP2/6-311++G** level of theory, and optimized structures of minima and saddle points are at the B3LYP/6-31G* level. Numbering refers to structures represented in Schemes 1−3.

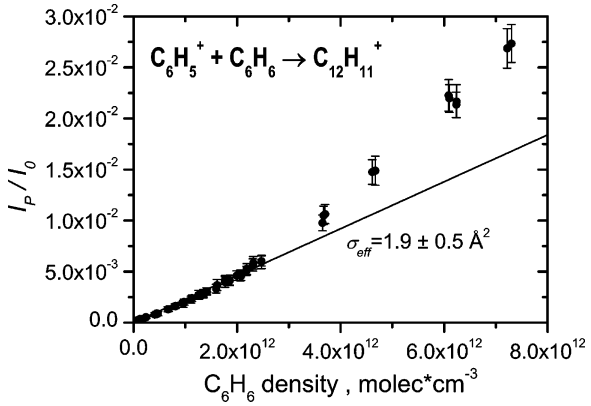

Figure 3. Density dependence of the $C_{12}H_{11}^+$ association product from the reaction of phenylium cation with benzene at collision energy E_{cm} = 0.23 eV. The solid line is the linear fit of data in the low-density regime, from which a value of 1.9 ± 0.5 Å^2 is obtained for the effective bimolecular association cross section.

4.1. $C_{12}H_{11}^+$. Products at *m*/*z* 155 correspond to the adduct $C_{12}H_{11}^+$ of phenylium with benzene (see Scheme 1). The most plausible structure for such species corresponds to protonated biphenyl,[26] in contrast with a previous proposal of a monocylic structure of the type phenylhexatriene.[27] In support of the protonated biphenyl structure is also the study of the surface induced dissociation reaction of $C_{12}H_{11}^+$.[28] Assuming protonated biphenyl as the final product, the energetics of the addition reaction, using NIST values,[29] is

$$C_6H_5^+ + C_6H_6 \rightarrow C_{12}H_{11}^+ \qquad \Delta H_r^o = -3.38\text{eV} \quad (8)$$

Our theoretical calculations indicate that the most stable structure of protonated biphenyl is species **4** in Scheme 1, which lies 3.5 eV lower in energy with respect to reagents. A schematic energy profile is reported in Figure 2, and the molecular structures of the relevant stationary points are shown in Schemes 1−3. The pathway leading to **4** is barrierless and proceeds through a direct association of a benzene molecule on the ipso carbon of the phenylium ion to give the intermediate complex **1** (at 2.9 eV below reagents), followed by a series of isomerization reactions to structures **2**, **3**, and **4** (see Figure 2, solid lines). We note in passing that our calculated relative stabilities of structures **1**−**4** are in good agreement with calculations of absolute proton affinities of biphenyl.[30]

SCHEME 1: Schematic Pathways Leading from $C_6H_5^+ + C_6H_6$ Reagents to $C_{12}H_{11}^+$ in All Its Different Isomers 1−4[a]

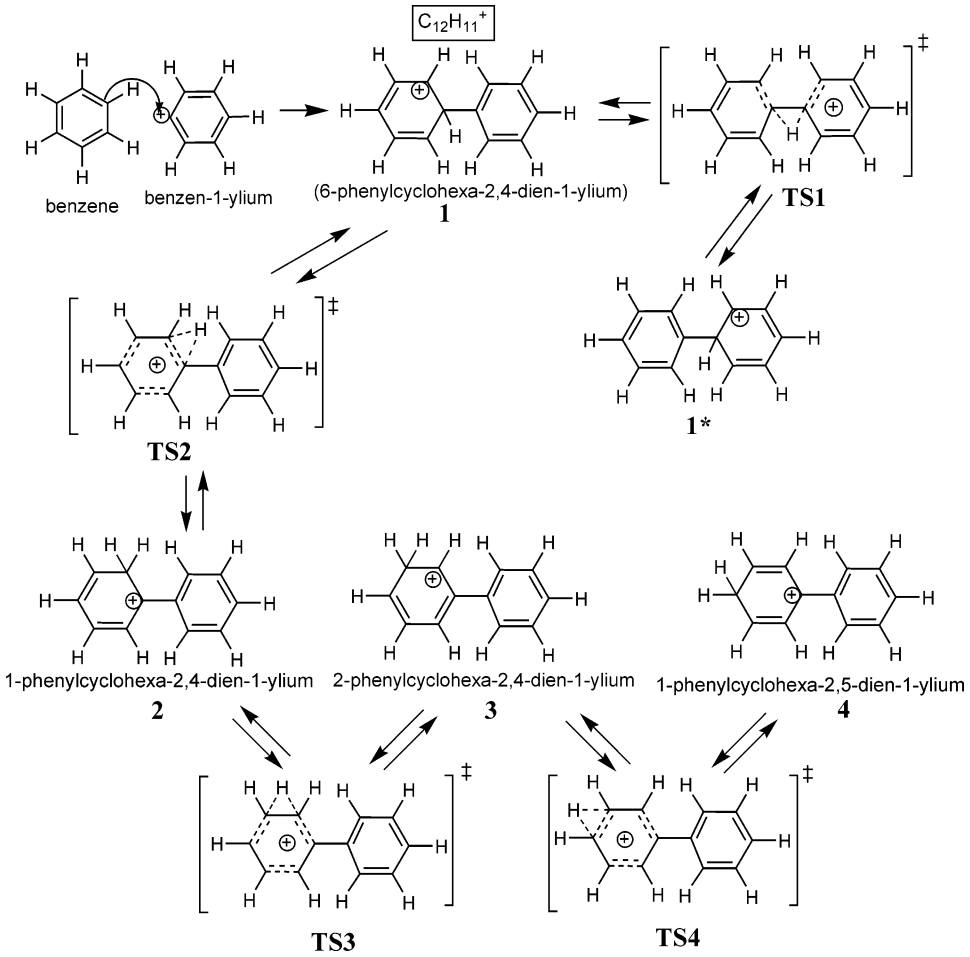

[a] For the energetics see Figure 2.

SCHEME 2: Schematic Description of the Two Possible Pathways for the Reaction Channel Producing $C_{12}H_9^+ + H_2$[a]

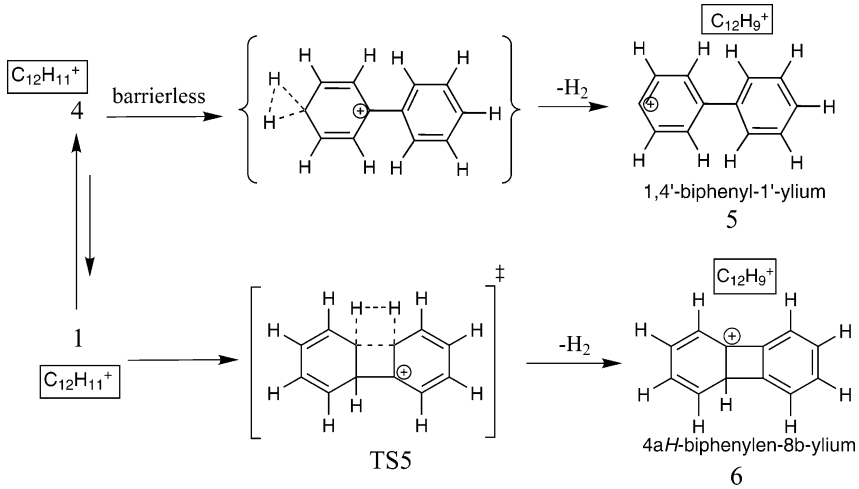

[a] Isomer **5** of $C_{12}H_9^+$ corresponds to a phenyl-substituted phenylium ion and can be produced via a barrierless elimination of H_2 from complex **4** (process **4**−**5**). Isomer **6** corresponds to a protonated biphenylene cation and can be produced from complex **1** via the transition state **TS5** (process **1**−**6**). for the energetics see Figure 2.

The production of the associated complex $C_{12}H_{11}^+$ has been studied by measuring the ratio I_P/I_0 as a function of the density of benzene in the reaction cell, and results are shown in Figure 3 for a center-of-mass collision energy $E_{cm} = 0.23$ eV. Data are linear with density up to a value $\sim 3 \times 10^{12}$ molecules·cm^{-3} (corresponding to a pressure of $\sim 1.2 \times 10^{-4}$ mbar) and ions formed under low-pressure conditions derive from a single-collision association process, in which the collision complex is stabilized either by IVR (intramolecular vibrational relaxation) or by radiative emission of an IR photon. At higher gas densities the quadratic contribution becomes dominant because, in the high-pressure regime, $C_{12}H_{11}^+$ production is the result of

SCHEME 3: Schematic Pathway for the Reaction Channel Producing $C_{10}H_9^+$ (Isomer 9, Protonated Naphthalene) + C_2H_2 Starting from $C_{12}H_{11}^+$ in the Isomer 1 Structure[a]

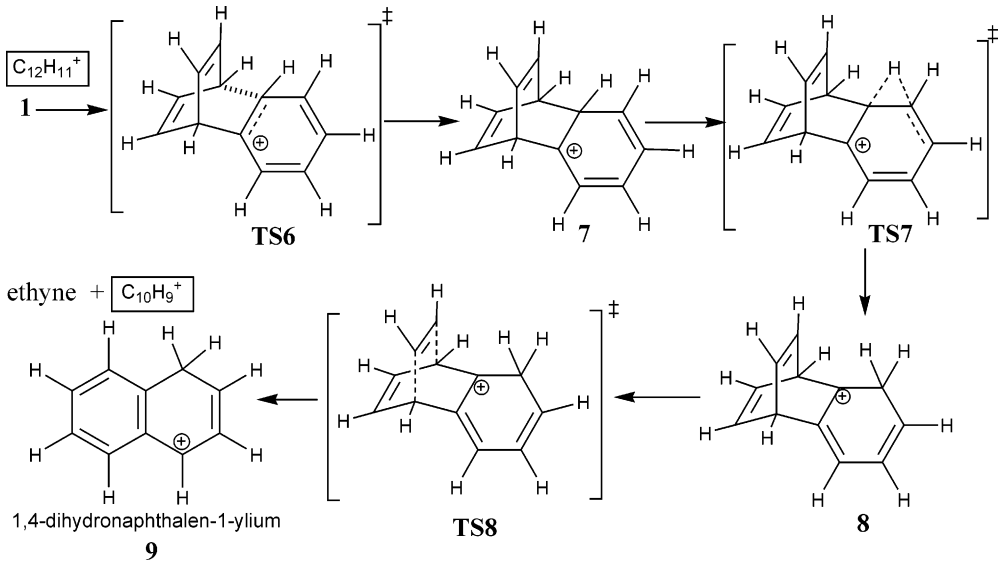

[a] See Figure 2 for the energies of transition states and intermediates.

collision-induced stabilization processes. From the best fit of data in the low-pressure region a value of 1.9 ± 0.5 Å^2 is derived for the absolute value of the cross section for production of $C_{12}H_{11}^+$.

Integral cross sections for reaction 8 are shown in Figure 4 over the center-of-mass collision energy E_{cm} range from 0.2 to 3 eV. Data have been collected with a C_6H_6 pressure in the scattering cell in the range $(2-5) \times 10^{-5}$ mbar to ensure adduct production via bimolecular association. The absolute value of the cross section has been measured, as described in section 2, at two collision energies ($E_{cm} = 0.23$ and 0.7 eV), and data are shown as open dots. Cross sections at the other collision energies have been rescaled accordingly.

In Figure 4 we have also reported cross section values σ obtained from rate constants k measured at thermal energies[16,21,22] and transformed as $k = \langle \sigma v \rangle$, where v is the relative velocity. Our data at lower collision energies compare well with data at thermal energies. In the energy range 0.2−1 eV we observe a decrease of the cross section as the collision energy increase which fits with a $E_{cm}^{-1.3}$ dependence. At energies >1 eV the complex formation channel is suppressed by collision energy (exhibiting an exponential decay). The energy dependence should be related to the lifetime of the complex and the amount of energy that can be redistributed into its internal degrees of freedom.

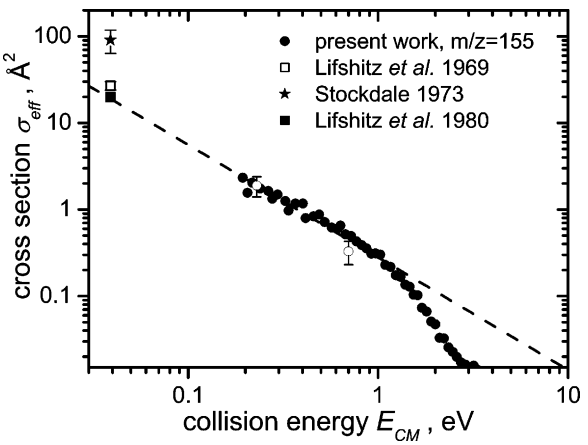

Figure 4. Cross sections as a function of the collision energy E_{cm} for reaction 8 leading to $C_{12}H_{11}^+$, shown as solid circles. The dashed line is a guide for the eye, which indicates a dependence $E_{cm}^{-1.3}$. Literature data at thermal energies: □, ref 22; ★, ref 16; ■, ref 21.

4.2. $C_{12}H_{10}^+$ and $C_{12}H_9^+$. Products at *m*/*z* 154 and 153 correspond to $C_{12}H_{10}^+$ and $C_{12}H_9^+$ ions, respectively, coming from the elimination of an H atom or an H_2 molecule from the adduct. Assuming that the $C_{12}H_{10}^{+\bullet}$ has the structure of the biphenyl radical cation, the energetics is

$$C_6H_5^+ + C_6H_6 \rightarrow C_{12}H_{10}^{+\bullet} + H \qquad \Delta H_r^o = +0.73 \text{ eV} \quad (9)$$

as obtained by MP2/6-311++G**//B3LYP/6-31G* calculations. It is worth noting that the corresponding value at B3LYP/6-31G* level is −0.39 eV, in perfect agreement with the value obtainable from NIST data.[29] Reasons for such a discrepancy are unclear.

$C_{12}H_9^+$ ions formed by ionization of a benzene cluster beam[28] have been assumed to have the structure of a phenyl-substituted phenylium ion (isomer **5** in Scheme 2). It is possible to estimate the value for the heat of formation (ΔH_f^0) of $C_{12}H_9^+$ assuming the loss of an H atom from the biphenyl radical cation $C_{12}H_{10}^{+\bullet}$.[31] Taking D(C−H) and IE($C_{12}H_{10}$) to be 4.6 and 8.16 eV, respectively, $\Delta H_f^0(C_{12}H_9^+)$ is found to be ∼12.7 eV. Using such values, the dehydrogenation channel is almost thermoneutral:

$$C_6H_5^+ + C_6H_6 \rightarrow C_{12}H_9^+ + H_2 \qquad \Delta H_r^0 = 0 \text{ eV} \quad (10)$$

Our calculations for the process **4**→**5** (Scheme 2) are in nice agreement with this estimate ($\Delta H_r^0 = -0.02$ eV; see Figure 2).

Alternatively, $C_{12}H_9^+$ might have the structure of a protonated biphenylene cation (our calculations indicate isomer **6** in Scheme 2 as the most stable isomer). Using NIST data[29] for ΔH_f^0, IE, and PA of biphenylene $C_{12}H_8$, a value of 11.4 eV is found for $\Delta H_f^0(C_{12}H_9^+)$, and reaction $C_6H_5^+ + C_6H_6 \rightarrow$ **1** → **6** (Scheme 2) would be exothermic by 1.3 eV. Our calculations of such a process give a value of 1.13 eV for the exothermicity. However, the reaction is calculated to proceed via the transition state **TS5** (see Figure 2). The corresponding barrier results to be 0.34 eV at the MP2/6-31++G**//B3LYP/6-31G* level of theory,

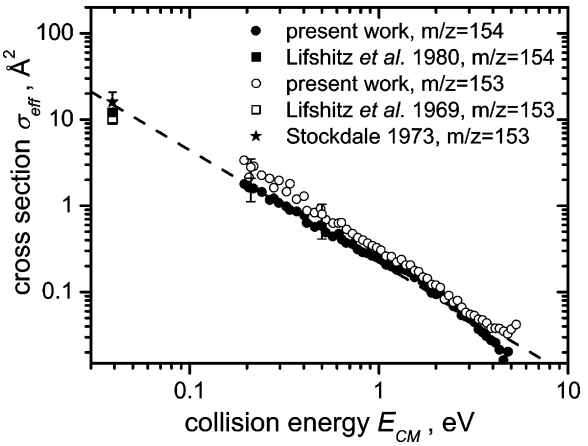

Figure 5. Cross sections as a function of the collision energy E_{cm} for reactions leading to $C_{12}H_{10}^+$ and $C_{12}H_9^+$, shown as solid and open circles, respectively. Dashed line is a guide for the eye which indicates a $E_{cm}^{-1.3}$ dependence. Literature data at thermal energies: ■, m/z = 154;[21] □, m/z = 153;[22] ★, m/z = 153.[16]

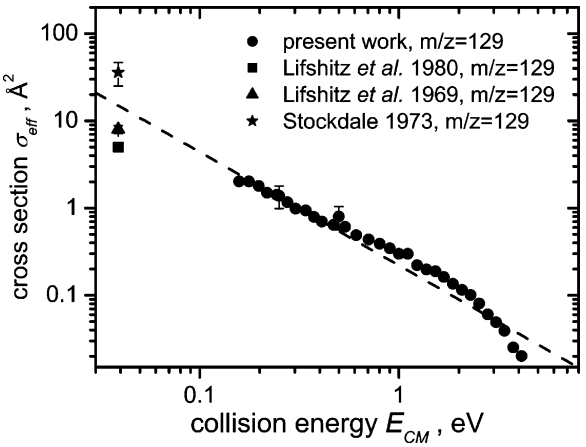

Figure 6. Cross sections as a function of the collision energy E_{cm} for reactions leading to $C_{10}H_9^+$, shown as solid circles. The dashed line is a guide for the eye which indicates a $E_{cm}^{-1.3}$ dependence as reported in Figure 4. Literature data at thermal energies: ■, ref 21; ▲, ref 22; ★, ref 16.

whereas it is 1.15 eV at the B3LYP/6-31G* level. No matter their reliability, calculations at both levels of theory give some hints that the barrier from **1** to **6** is high enough to rule out a significant formation of **6** via **TS5**, unless tunneling effects are relevant. Alternatively, the less stable phenyl-substituted phenylium ion (structure **5**) might isomerize into the protonated biphenylene cation (structure **6**) via (1,6) hydrogen transfer and successive C−C bond formation. Energy barriers for such a process should be low and therefore it might be possible that the observed $C_{12}H_9^+$ ion is actually protonated biphenylene. Calculations at a higher level of theory would be necessary to clarify this point.

Integral cross sections for the H and H_2 elimination channels (9) and (10) are shown in Figure 5 as solid and open circles over the center-of-mass collision energy E_{cm} range from 0.2 to 5 eV. Experimental conditions and calibration of the absolute value of the cross sections are similar to $C_{12}H_{11}^+$. The elimination of molecular H_2 is favored over the entire energy range, and in both cases cross sections show a negative energy dependence which can be described as a decay of the type $E_{cm}^{-1.3}$, similar to what observed in the $C_{12}H_{11}^+$ case at E_{cm} < 1 eV. At E_{cm} > 1 the probability of the fragmentation channels becomes higher than that for adduct formation. In the case of $C_{12}H_{10}^+$ products, the absence of a threshold in the cross section speaks for a barrierless exothermic process and therefore supports B3LYP/6-31G* results. Furthermore, the similarity in the energy dependence of the cross sections for $C_{12}H_{11}^+$ and the elimination channels suggests that the latter might be complex-mediated, i.e., they proceed via formation and subsequent fragmentation of the $C_{12}H_{11}^+$ adduct, with complex formation probability and/or lifetime that are strongly suppressed by E_{cm}. Two experimental evidences support the complex-mediated mechanicistic hypothesis: (a) when working with mixed isotopic reagent pairs, extensive H/D atom scrambling is observed on the fragmentation products (see section 4.5); (b) MS/MS spectra of the adducts $C_{12}H_{11}^+$, $C_{12}H_5D_6^+$, and $C_{12}D_5H_6^+$ generated in the APCI source from a 1:1 mixture of benzene and benzene-d_6 show a fragmentation pattern that resembles the one observed in the GIB-MS experiment and shown in Figure 1 (see section 4.5).

4.3. $C_{10}H_9^+$. Products at m/z 129 correspond to $C_{10}H_9^+$ ions, resulting from the loss of an ethyne (acetylene) molecule by the condensation product $C_{12}H_{11}^+$. The elimination of a C_2H_2 neutral is a well-established fragmentation process for aromatic molecular ions and has been observed previously.[11,16,20−22] Assuming that the $C_{10}H_9^+$ has the structure of protonated naphthalene, and using the available thermochemical data,[29] the energetics of the loss channel is

$$C_6H_5^+ + C_6H_6 \rightarrow C_{10}H_9^+ + C_2H_2 \qquad \Delta H_r^0 = -1.25 \text{ eV} \tag{11}$$

Results of our calculations for the intermediate adducts and transition states leading to acetylene loss are shown in Figure 2 as dashed-dotted lines. In nice agreement with the thermochemical data, the formation of protonated naphthalene is calculated to be exothermic by 1.27 eV. As outlined in Scheme 3, reaction **1**→**9** proceeds from the protonated biphenyl adduct (isomer **1**) which rearranges into the intermediate **7** via **TS6**, with an activation energy below the reactant energy. Generation of **7** from isomers **1**/**1*** requires the formation of a tetracyclic 6-member ring system through an intermolecular electrophilic attack of the phenyl moiety on the benzene one. Isomer **7** rearranges into **8** via **TS7** by 1,2 H shift. The elimination of an ethyne molecule from **8** requires the rupture of two C−C bonds via the transition state **TS8**. Overall, the intermediate complexes and transition states for reaction **1**→**9** in Scheme 3 are at energies below those of the reactants. Again, we must outline that **TS8**, which lies below the reactants at MP2/6-311++G**//B3LYP/6-31G* level of theory, results instead above them by 0.2 eV at B3LYP/6-31G* level.

The integral cross section for the acetylene elimination channel is shown in Figure 6 over the center-of-mass collision energy E_{cm} range from 0.2 to ∼ 5 eV. Experimental conditions and calibration of the absolute value of the cross sections are similar to $C_{12}H_{11}^+$. The cross section shows a negative energy dependence that is similar to what observed in the $C_{12}H_{11}^+$ case at E_{cm} < 1 eV (shown as dashed line in Figure 6), thus supporting MP2 results.

Both experiments and theory show that the reaction of phenylium ions with benzene leads to the synthesis of naphthalene, the smallest PAH, via a barrierless pathway. Therefore, this reaction might be relevant for the production of condensed aromatic rings in environments, such as Titan's ionosphere, where benzene and its ions are present.[32,33]

4.4. $C_9H_7^+$. Products at m/z 115 correspond to $C_9H_7^+$ ions resulting from a considerable rearrangement of bonds in the reagents leading to the overall loss of a neutral C_3H_4 (most likely

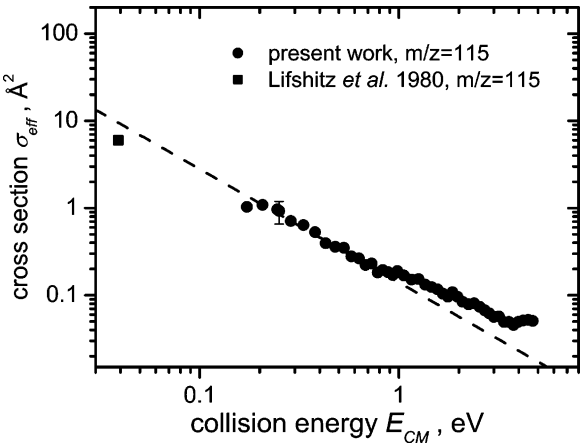

Figure 7. Cross sections as a function of the collision energy E_{cm} for reactions leading to $C_9H_7^+$ are shown as solid circles. The dashed line is a guide for the eye which indicates a $E_{cm}^{-1.3}$ dependence as reported in Figure 4. Literature data at thermal energy: ■, ref 21.

with an allene structure $CH_2{=}C{=}CH_2$). The most stable structure for the ion $C_9H_7^+$ is [indene − H]$^+$. The reaction of phenylium cation with benzene leading to $C_9H_7^+$ was observed also in ICR mass spectrometry experiments:[20] on the basis of thermochemical data available at the time, the reaction was assumed to be endothermic by about 0.4 eV and past speculations have invoked the reaction of internally or translationally excited $C_6H_5^+$ ions. Assuming the formation of the indenyl ion structure, we have re-evaluated the thermochemistry using updated thermochemical data (i.e., $\Delta H_f^0(C_9H_7^+) = 10.4$ eV[34] and $\Delta H_f^0(C_3H_4) = 1.975$ eV[35]) and we have found that the energetics is

$$C_6H_5^+ + C_6H_6 \rightarrow C_9H_7^+ + C_3H_4 \qquad \Delta H_r^0 = -0.4 \text{ eV} \tag{12}$$

Our calculations give a value of −0.03 eV at the MP2/6-311++G**//B3LYP/6-31G* level of theory and −0.26 eV at the B3LYP/6-31G* level.

The integral cross section for the production of $C_9H_7^+$ is shown in Figure 7 over the center-of-mass collision energy E_{cm} range from 0.2 to ∼5 eV. Experimental conditions are similar to $C_{12}H_{11}^+$, and the absolute value of the cross section has been measured at $E_{cm} = 0.25$ eV. The cross section dependence on the collision energy shows that, once again, product is formed mainly at low collision energies and therefore it should derive either from an exothermic process or from the reaction of excited phenylium cations. To investigate the role of internal excitation of phenylium ion we have measured the amount of $C_9H_7^+$ ions produced under different conditions in the ion source, specifically with and without He in the cooling octopole. Results are shown in Figure 8: there is a decrease of a factor 1.3 in the amount of $C_9H_7^+$ produced when He is added to the first octopole, while the amount of $C_{10}H_9^+$ remains the same. We believe this is an indication that internally excited phenylium ions play a role in the production of $C_9H_7^+$.

4.5. H/D Scrambling. Inter-ring scrambling in bicyclic aromatic systems such as biphenyl has been observed in the past. The fragmentation reactions of the biphenyl-2,3,4,5-d_5 cation were studied and it was found that H and D atoms are to a large degree randomized over both rings prior to fragmentation.[36] Statistical scrambling has been observed in the MIKE spectra of $[C_{12}(H,D)_{11}]^+$ species formed by admitting a 1:1 mixture of C_6H_6 and C_6D_6 in an ion source at intermediate pressure (∼0.7 mbar).[27]

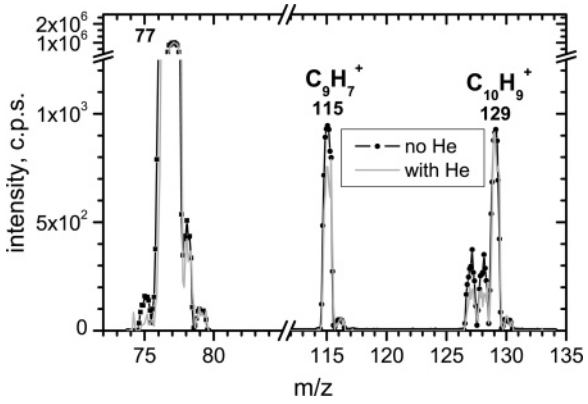

Figure 8. Mass spectra of reagent ($m/z = 77$) and product ions at $m/z = 115$ $m/z = 129$ with and without the addition of He in the cooling octopole. The collision energy is $E_{cm} = 0.46$ eV and benzene pressure in the reaction cell is 5×10^{-5} mbar.

We have performed experiments in an APCI source coupled with an ion trap mass spectrometer. Working with a 1:1 mixture of benzene and benzene-d_6 in the ion source we have observed the presence of the fully hydrogenated $C_{12}H_{11}^+$ (m/z 155), the fully deuterated $C_{12}D_{11}^+$ (m/z 166), and the partially deuterated $C_{12}D_5H_6^+$ (m/z 160) and $C_{12}H_5D_6^+$ (m/z 161) ions, as expected from the reactivity of $C_6H_5^+$ and $C_6D_5^+$ ions with their precursors. MS/MS experiments on the partially deuterated ions have been carried out by resonant activation of such ions with the He gas present in the trap and via collision induced dissociation measurements, and results are shown in Figure 9. The MS/MS spectrum of the $C_{12}H_{11}^+$ ion at m/z 155 shows a fragmentation pattern in which the most intense ionic fragments occur at m/z 154 (loss of H atom), 153 (loss of H_2), 129 (loss of C_2H_2), 115 (loss of C_3H_4), and 77 (loss of C_6H_6). It is interesting to note that all such ions have also been observed as products of the reaction between $C_6H_5^+$ and C_6H_6 in the GIB-MS setup. This is a further element in favor of a complex-mediated mechanism according to which the reaction proceeds via formation of a long-lived intermediate complex $C_{12}H_{11}^+$ from which several dissociation channels exist to produce ions $C_{12}H_{10}^+$, $C_{12}H_9^+$, $C_{10}H_9^+$, $C_9H_7^+$, and $C_6H_5^+$. The MS/MS spectra of the partially deuterated complexes $C_{12}D_5H_6^+$ and $C_{12}H_5D_6^+$ show the same fragmentation channels, complicated by the fact that for each daughter ion several H/D combinations are possible (e.g., molecular hydrogen loss can occur as H_2, HD or D_2). The fragmentation channel that is most congenial to analysis is the loss of $C_3(H,D)_4$, because daughter ions occur in regions virtually free of other ions. On the contrary, the H,D and $(H,D)_2$ elimination channels are complicated by mass overlap of different fragmentation channels (i.e., in the case of MS/MS over m/z 161, $C_{12}H_5D_5^+$ and $C_{12}H_3D_6^+$ both appearing at m/z 159) and the same is, to a less extent, true for the acetylene loss channel. In the absence of scrambling, the exclusive loss of C_3H_4 and C_3D_4 should be observed. Fragmentation by loss of $C_3(H,D)_4$ leads instead to a cluster of ions peaked at m/z 118 for $C_{12}D_5H_6^+$ (m/z 160) and at m/z 119 for $C_{12}H_5D_6^+$ (m/z 161), as shown in the two bottom panels of Figure 9. The intensities within each cluster are compatible with those expected from a complete scrambling of H and D atoms over both rings prior to fragmentation.

To further investigate the H/D atom scrambling occurring during the reactions of phenylium cations with benzene, we have recorded mass spectra within the GIB-MS setup using the $C_6H_5^+ + C_6D_6$ and $C_6D_5^+ + C_6H_6$ isotope combinations. In both cases mass spectra are complicated by an extensive atom scrambling (see Figure 10 for the $C_6H_5^+/C_6D_6$ reagent pair), which implies

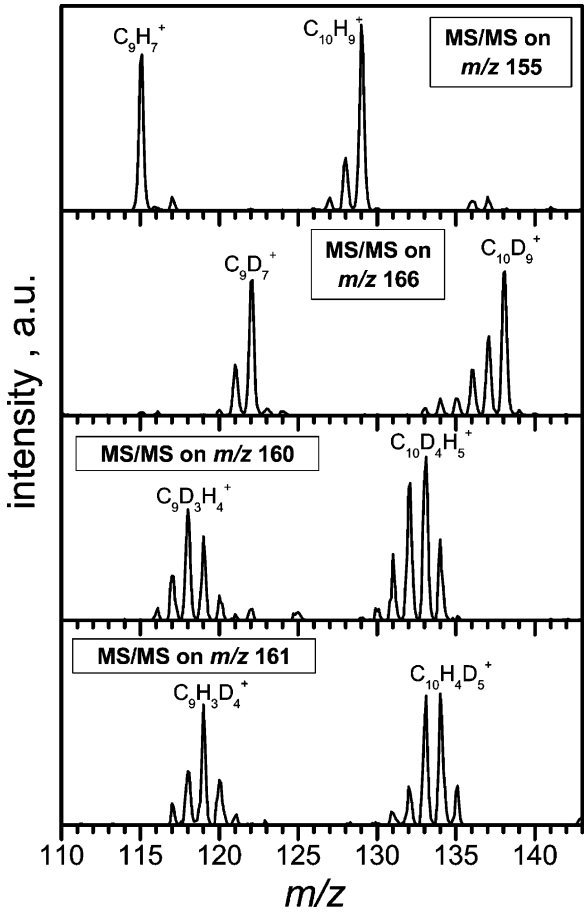

Figure 9. MS/MS spectra of the various C_{12} $(H,D)_{11}^+$ ions formed inside the APCI source from 1:1 mixtures of C_6H_6 and C_6D_6. Data are shown in the mass range 110−143 to highlight the spectral region where $C_9(H,D)_7^+$ fragments occur.

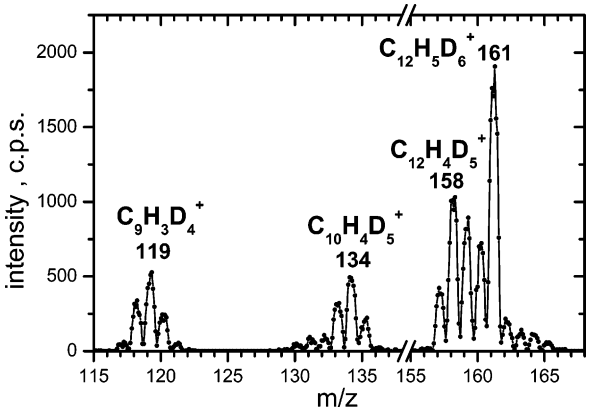

Figure 10. Mass spectrum of product ions resulting form the reaction of $C_6H_5^+$ with C_6D_6 in the GIB-MS setup. The collision energy is E_{cm} = 0.27 eV and benzene-d_6 pressure in the reaction cell is 5.6×10^{-5} mbar.

the formation of a long-lived collision complex as well as the occurrence of extensive rearrangements prior to fragmentation. Even in this case, we have looked at the relative intensities of products corresponding to the elimination of $C_3(H,D)_4$ from both mixed reagent pairs. This is shown in Figure 11 where the observed intensities are compared with the calculated intensities that would be expected if randomization of the H and D positions had occurred in the complex prior to production of $[C_9(H,D)_7]^+$. In the calculation, allowance has been made for the presence of ^{13}C at natural abundance and peak intensities have been normalized to give a total intensity of 100.0.

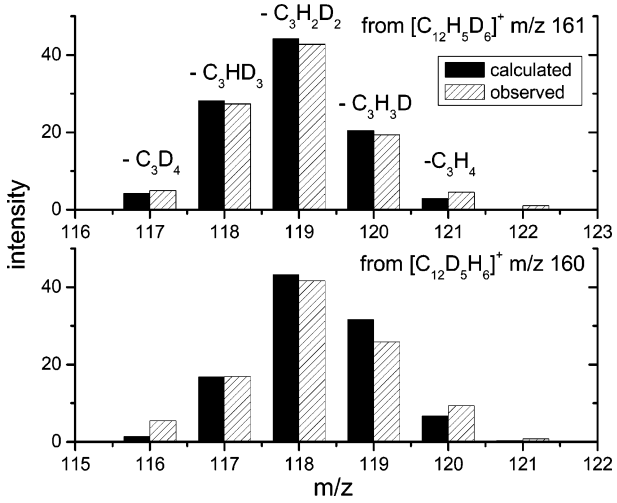

Figure 11. Observed and calculated intensities for randomization of position of H and D atoms from the ions corresponding to the loss of $C_3(H,D)_4$ from $[C_{12}H_5D_6]^+$ and $[C_{12}D_5H_6]^+$ generated from the reagent pairs $C_6H_5^+/C_6D_6$ and $C_6HD_5^+/C_6H_6$, respectively. In all cases the total ion intensity for the fragmentation channels has been set equal to 100.0.

Calculated and experimental intensities are in close agreement, suggesting that the mechanism for formation of the $[C_9(H,D)_7]^+$ ion involves the production of a $[C_{12}(H,D)_{11}]^+$ adduct where the H and D atoms are randomized over both rings.

Gaseous arenium ions such as those of benzene and naphthalene are known to undergo statistical H/D scrambling as a consequence of the significant mobility of hydrogen atoms along the aromatic rings.[23,24] Present experimental results indicate that this is the case also for protonated biphenyl structures. For the hydrogen scrambling to be complete over both rings, the energy barriers to 1,2-hydrogen shift both intra- and inter-ring should be small and of similar magnitudes. As shown in Figure 2 and Scheme 1, the intra-ring H shift from isomer **1** to **2** proceeds via a transition state **TS2**, which gives a barrier of 0.1 eV. Subsequent intra-ring H shifts lead to structure **3** via transition state **TS3** (barrier 0.5 eV) and to the most stable isomer **4** via **TS4** (barrier 0.2 eV). By inter-ring shifting of an H atom, **1** evolves into **1*** via **TS1** and this isomerization process requires 0.6 eV.

Due to the energy difference between **TS1** and **TS2**, H atoms would prefer "walking'' along one aromatic ring and this would lead to non-statistical scrambling. However, the strong exothermicity for formation of adduct **1** makes so much energy available that products are formed with statistical yields.

4.6. $C_6H_n^+$ Products, with n = 5, 6. Reaction products containing six C atoms and either five or six H atoms can derive from charge exchange or back-fragmentation of the $C_{12}H_{11}^+$ adduct into the reactants. To investigate such channels, we have used the $C_6H_5^+ + C_6D_6$ and $C_6D_5^+ + C_6H_6$ isotope combinations, and spectra of products in the C_6 mass region are reported in Figure 12.

1. Back-Fragmentation with H/D Scrambling. Products at *m/z* 80 in the $C_6H_5^+/C_6D_6$ reactive pair and products at *m/z* 79 in the $C_6D_5^+/C_6H_6$ case are the most intense product channels containing six C atoms. Most likely they correspond to $C_6H_2D_3^+$ (*m/z* 80) and $C_6D_2H_3^+$ (*m/z* 79) coming from back-fragmentation of the reagents after H/D scrambling, even though a contribution from the isobaric ions with formula $C_6(H,D)_6^+$ might be possible (i.e., $C_6H_4D_2^+$ at *m/z* 80 and $C_6H_5D^+$ at *m/z* 79). As a matter of fact, the production of $C_6(H,D)_6^+$ can be excluded on the following basis:

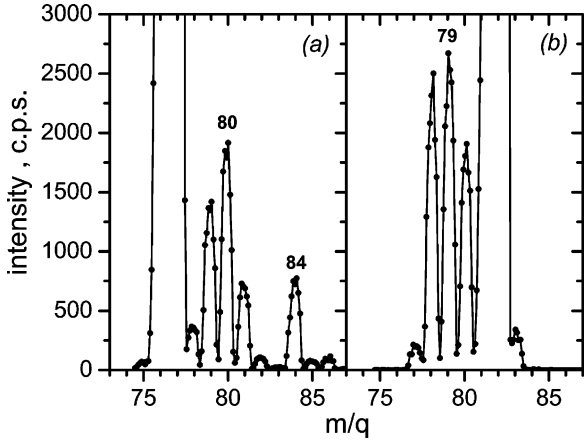

Figure 12. Mass spectra of product ions containing six C atoms from the reaction of $C_6H_5^+ + C_6D_6$ (a) and $C_6D_5^+ + C_6H_6$ (b). The collision energy is $E_{cm} \sim 0.6$ eV in both cases. Benzene and benzene-d_6 pressures in the reaction cell are in the range $(2-6) \times 10^{-5}$ mbar.

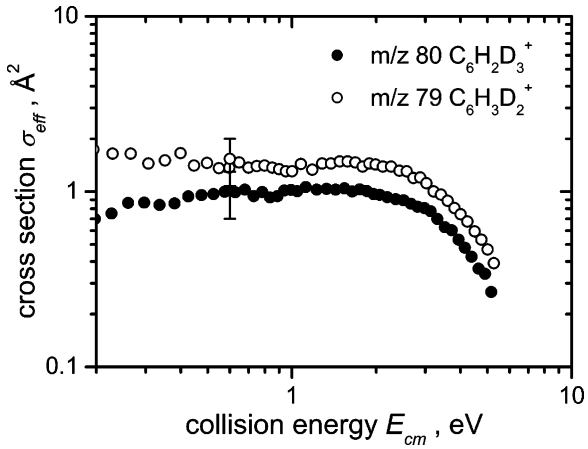

Figure 13. Cross sections as a function of the collision energy E_{cm} for reactions leading to *m*/*z* 80 and *m*/*z* 79 using the reagent pairs $C_6H_5^+/C_6D_6$ and $C_6D_5^+/C_6H_6$, respectively.

(1) If product at *m*/*z* 79 were due to $C_6H_5D^+$, when the reversed isotopic mixture of reagent $C_6H_5^+/C_6D_6$ was used, the same product should appear as $C_6D_5H^+$ at *m*/*z* 83. However, it is clear from Figure 12a, that no product is observed at such an *m*/*z* value.

(2) The energy dependence of the integral cross sections for the ion products at *m*/*z* 80 and 79 is similar, being almost independent of energy up to about 2 eV and showing a negative dependence at higher energies, as reported in Figure 13. This is further evidence that both products correspond to the same chemical species.

Absolute values of the cross sections for both channels have been measured independently as described in the Experimental Section at a collision energy $E_{cm} = 0.6$ eV.

The reactive processes reported in Figure 13 correspond to

$$C_6(H,D)_5^+ + C_6(D,H)_6 \rightarrow C_6(H,D)_2(D,H)_3^+ + C_6H_3D_3 \quad (13)$$

in which three H atoms have been scrambled with three D atoms (or vice versa). For the scrambling to be feasible, the formation of the $C_6(H,D)_2$ $(D,H)_3^+$ ions should proceed via the production of the $C_{12}(H,D)_{11}^+$ adduct as a reaction intermediate. Different from what is observed for the other fragmentation channels giving $C_{12}H_{10}^+$, $C_{12}H_9^+$, $C_{10}H_9^+$, and $C_9H_7^+$, the cross section for back-fragmentation does not show a negative energy dependence up to $E_{cm} \sim 2$ eV. This can be explained assuming that the translational energy plus the exothermicity for the formation of the adduct is efficiently redistributed over two fragments having similar masses.

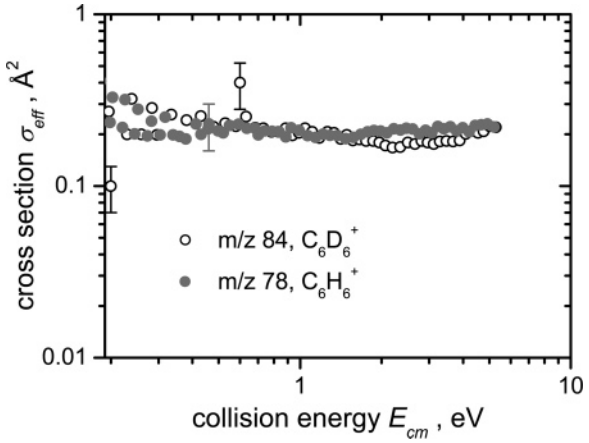

Figure 14. Cross sections as a function of the collision energy E_{cm} for the charge-transfer channels leading to *m*/*z* 78 and *m*/*z* 84 using the reagent pairs $C_6H_5^+/C_6H_6$ and $C_6H_5^+/C_6D_6$, respectively.

2. Charge-Transfer Channel. The charge exchange channel

$$C_6H_5^+ + C_6(H,D)_6 \rightarrow C_6H_5 + C_6(H,D)_6^+ \quad (14)$$

is one of the minor channels in the reactive system under study. However its formation has been observed either as $C_6H_6^+$ at *m*/*z* 78 when working with $C_6H_5^+/C_6H_6$ or as $C_6D_6^+$ at *m*/*z* 84 in the $C_6H_5^+/C_6D_6$ case. Cross sections are shown in Figure 14: the energy dependence for the ion products at *m*/*z* 78 and 84 is similar, being practically independent of the collision energy in the whole range explored by our measurements (from 0.2 to 5 eV).

In the $C_6H_5^+/C_6D_6$ case, the absolute value of the cross section for process (14) has been indirectly determined from a comparison of the relative abundances of ions at *m*/*z* 80 (for which a direct measurement of the absolute value of the cross section was available) and 84 taken from mass spectra recorded at two collision energies ($E_{cm} = 0.2$ and 0.6 eV). In this way values of 0.1 and 0.4 Å^2 are obtained respectively at $E_{cm} = 0.2$ and 0.6 eV, and results are shown as the open circles in Figure 14 with error bars corresponding to30% . Due to the well-known uncertainties in the collection efficiencies of backscattered products using the guided ion beam technique, the above-mentioned value is a lower limit for the charge-transfer cross section. The cross sections at the other collision energies have been rescaled to be within the two above-mentioned values. In the $C_6H_5^+/C_6H_6$ case, the absolute value of the cross section for *m*/*z* 78 has been obtained from a comparison of the relative abundances of ions at *m*/*z* 78 and at *m*/*z* 115, 129, 153, 154, and 155 (for all such ions direct measurements of the absolute value of the cross section were available) taken from a mass spectrum recorded at $E_{cm} = 0.46$ eV. A value of 0.2 Å^2 is obtained and it is shown as the filled circle with a 30% error bar in Figure 14. Within the sensitivity of our experiment, the charge trasfer cross sections have the same asbolute value when using C_6H_6 or C_6D_6 as target gases.

3. H^-/D^- Abstraction Channel. When working with the isotopic reagent pair $C_6D_5^+/C_6H_6$ the following reactive channel is observed,

$$C_6D_5^+ + C_6H_6 \rightarrow C_6H_5^+ + C_6D_5H \quad (15)$$

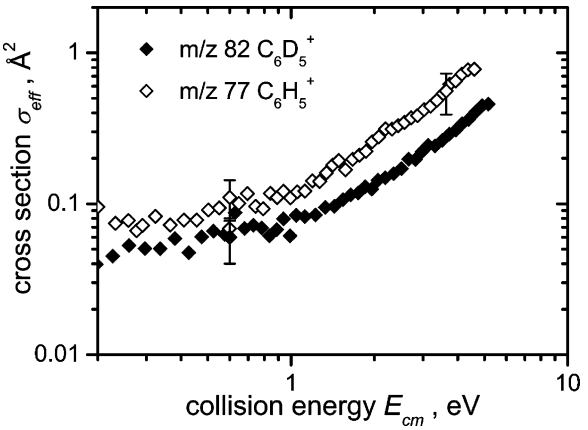

Figure 15. Cross sections as a function of the collision energy E_{cm} for reactions leading to *m*/*z* 77 and *m*/*z* 82 using the reagent pairs $C_6D_5^+/C_6H_6$ and $C_6H_5^+/C_6D_6$, respectively.

by measuring the amount of product at *m*/*z* 77. Unlike the other products, the reactive cross section for this channel increases with the collision energy: because product formation is maximized at high collision energies (see Figure 15, open diamonds), it cannot derive from fragmentation of the adduct $C_{12}(H,D)_{11}^+$. The same reactive channel, with a similar dependence on the collision energy, is also observed when working with $C_6H_5^+/C_6D_6$ at *m*/*z* 82 and reactive cross section as a function of the collision energy are shown in Figure 15 as filled diamonds:

$$C_6H_5^+ + C_6D_6 \rightarrow C_6D_5^+ + C_6H_5D \qquad (16)$$

In the $C_6D_5^+/C_6H_6$ case, the absolute value of the cross section for process 15 has been indirectly determined from a comparison of the relative abundances of ions at *m*/*z* 79 (for which a direct measurement of the cross section was available) and 77 at a collision energy $E_{cm} = 3.6$ and 0.6 eV (see the mass spectrum reported in Figure 12b). In a similar manner, in the $C_6H_5^+/C_6D_6$ case, the absolute value of the cross section for process 16 has been obtained from a comparison of the relative abundances of ions at *m*/*z* 80 (for which a direct measurement of the cross section was available) and 82 at collision energy $E_{cm} = 0.6$ eV (see the mass spectrum reported in Figure 12a). Reactions 15 and 16 formally correspond to an overall H^- or D^- transfer from $C_6(H,D)_6$ to $C_6(D,H)_5^+$, but they could also derive from a dissociative charge-transfer process. However, were this the case, the corresponding charge-transfer channel (14) should show a decrease in the amount of products generated at high collision energy, due to the dissociation into $C_6(H,D)_5^+ + (H,D)$, but this is clearly not observed in Figure 14. The collision energy dependence is probably due to the presence of an energy barrier along the reaction path, in a process that is thermoneutral, apart from small differences in the zero-point energies of reactant and products due to different H/D isotope content.

5. Conclusions

We report a study on the reactivity of phenylium cations with benzene, by measuring both product yields as a function of benzene density, and absolute integral reactive cross sections as a function of the collision energy. At low collision energies the reactivity is dominated by the formation of a stable intermediate complex $C_{12}H_{11}^+$ having the structure of protonated biphenyls **1**−**4**, with a significant mobility of the H atoms over both rings. This has been demonstrated by the statistical H/D scrambling observed in the fragmentation products when using mixed isotopic reagent pairs $C_6H_5^+/C_6D_6$ and $C_6D_5^+/C_6H_6$. Loss of H and H_2 from the protonated biphenyls **1**−**4** leads to $C_{12}H_{10}^+$ and $C_{12}H_9^+$ ions. $C_{12}H_9^+$ might have structures **5** or **6**, the latter being more likely. The production of protonated naphthalene cation $C_{10}H_9^+$ via the barrierless elimination of an acetylene molecule from the intermediate complex has been inferred. Minor products have been observed as a result of charge-transfer processes and H^-/D^- abstraction, the latter being more probable at high collision energies.

It is worth of note that biphenyl can be produced in good yield from benzene chemical ionization at atmospheric pressure. In this case the coupling of two aromatic rings leading to biphenyl cation is produced according to a classical electrophilic aromatic substitution, wherein the phenyl cation $C_6H_5^+$ acts as a powerful attacking electrophile on a neutral benzene. Thus, the plasma producing $C_6H_5^+$ plays the same role of metal catalysts in the aryl−aryl bond formation, which is so important in modern organic synthesis.[6]

Acknowledgment. The technical assistance of Mr. Adriano Sterni during APCI mass measurements and of Dr. Damiano Avi for the guided ion beam measurements is greatly acknowledged. Funding for the present work was granted by the Department of Physics, University of Trento and by the Italian Government PRIN Contract No. 2005033911.

References and Notes

(1) Wang, H.; Frenklach, M. *Combust. Flame* **1997**, *110*, 173−221.
(2) Roithova, J.; Schroeder, D. *Phys. Chem. Chem. Phys.* **2007**, *9*, 731−738.
(3) Roithova, J.; Schroeder, D. *J. Am. Chem. Soc*. **2006**, *128*, 4208−4209.
(4) Ascenzi, D.; Franceschi, P.; Guella, G.; Tosi, P. *J. Phys. Chem. A* **2006**, *110*, 7841−7847.
(5) Franceschi, P.; Guella, G.; Scarduelli, G.; Tosi, P.; Dilecce, G.; Benedictis, S. D. *Plasma Proc. Polym.* **2007**, *4*, 548−555.
(6) Alberico, D.; Scott, M. E.; Lautens, M. *Chem. Rev.* **2007**, *107*, 174−238.
(7) Stuart, D. R.; Fagnou, K. *Science* **2007**, *316*, 1172−1175.
(8) Hassan, J.; Sevignon, M.; Gozzi, C.; Schulz, E.; Lemaire, M. *Chem. Rev.* **2002**, *102*, 1359−1469.
(9) LaVerne, J. A.; Araos, M. S. *J. Phys. Chem. A* **2002**, *106*, 11408−11413.
(10) Hentz, R. R.; Rzad, S. J. *J. Phys. Chem.* **1968**, *72*, 1027−1031.
(11) Lifshitz, C.; Reuben, B. G. *Isr. J. Chem*. **1969**, 7, *149*−152.
(12) Wexler, S.; Clow, R. P. *J. Am. Chem. Soc*. **1968**, *90*, 3940−3945.
(13) Park, J.; Lin, M. C. *J. Phys. Chem. A* **1997**, *101*, 14−18.
(14) Park, J.; Burova, S.; Rodgers, A. S.; Lin, M. C. *J. Phys. Chem. A* **1999**, *103*, 9036−9041.
(15) Park, J.; Burova, S.; Rodgers, A. S.; Lin, M. C. *Chem. Phys. Processes Combust.* **1999**, 308−311.
(16) Stockdale, J. A. D. *J. Chem. Phys.* **1973**, *58*, 3881−3883.
(17) Anicich, V. G.; Bowers, M. T. *J. Am. Chem. Soc*. **1974**, *96*, 1279−1284.
(18) Jones, E. G.; Bhattacharya, A. K.; Tiernan, T. O. *Int. J. Mass Spectrom. Ion Phys*. **1975**, *17*, 147−161.
(19) Sieck, L. W.; Gorden, R. J. *Int. J. Mass Spectrom. Ion Phys*. **1976**, *19*, 269−286.
(20) Smith, R. D.; Decorpo, J. J.; Futrell, J. H. *Int. J. Mass Spectrom*. **1978**, *26*, 279−288.
(21) Lifshitz, C.; Weiss, M. *Int. J. Mass Spectrom*. **1980**, *34*, 311−315.
(22) Lifshitz, C.; Reuben, B. G. *J. Chem. Phys*. **1969**, *50*, 951−960.
(23) Ascenzi, D.; Bassi, D.; Franceschi, P.; Tosi, P.; Stefano, M. D.; Rosi, M.; Sgamellotti, A. *J. Chem. Phys*. **2003**, *119*, 8366−8372.
(24) Ascenzi, D.; Bassi, D.; Franceschi, P.; Hadjar, O.; Tosi, P.; Stefano, M. D.; Rosi, M.; Sgamellotti, A. *J. Chem. Phys.* **2004**, *121*, 6728−6737.
(25) Ervin, K. M.; Armentrout, P. *J. Chem. Phys*. **1985**, *1*, 166−189.
(26) Wolfschuetz, R.; Schwarz, H. *Int. J. Mass Spectrom. Ion Phys.* **1980**, *33*, 285−290.
(27) Harris, J. A.; Morgan, R. P.; Beynon, J. H. *Org. Mass Spectrom.* **1979**, *14*, 4−8.
(28) Worgotter, R.; Mair, C.; Fiegele, T.; Grill, V.; Mark, T. D.; Schwarz, H. *Int. J. Mass Spectrom. Ion Processes* **1997**, *164*, L1−L6.

(29) National Institute of Standards and Technology, Gaithersburg, MD, 2005. URL http://webbook.nist.gov/chemistry/.

(30) Maksic, Z. B.; Baric, D.; Kovacevic, B. *J. Chem. Soc., Perkin Trans.* **1999**, *2*, 1011−1017.

(31) Natalis, P.; Franklin, J. L. *Int. J. Mass Spectrom. Ion Phys*. **1981**, *40*, 35−42.

(32) Waite, J. H., Jr.; Niemann, H.; Yelle, R. V.; Kasprzak, W. T.; Cravens, T. E.; Luhmann, J. G.; McNutt, R. L.; Ip, W.-H.; Gell, D.; Haye, V. D.; Muller-Wordag, I.; Magee, B.; Borggren, N.; Ledvina, S.; Fletcher, G.; Walter, E.; Miller, R.; Scherer, S.; Thorpe, R.; Xu, J.; Block, B.; Arnett, K. *Science* **2007**, 982−986; URL http://www.sciencemag.org/cgi/content/full/308/5724/982.

(33) Cravens, T. E.; Robertson, I. P.; Waite, J. H.; Yelle, R. V.; Kasprzak, W. T.; Keller, C. N.; Ledvina, S. A.; Niemann, H. B.; Luhmann, J. G.; McNutt, R. L.; Ip, W. H.; La, H. V. D.; Mueller-Wodarg, I.; Wahlund, J. E.; Anicich, V. G.; Vuitton, V. *Geophys. Res. Lett*. **2006**, *33*, L07105.

(34) Bouchoux, G.; Dagaut, J. *Org. Mass Spectrom*. **1982**, *17*, 151.

(35) Hayakawa, S.; Endoh, H.; Arakawa, K.; Morishita, N. *Int. J. Mass Spectrom*. **1997**, *171*, 209−214.

(36) Cooks, R. G.; Howe, I.; Tam, S.; Williams, D. H. *J. Am. Chem. Soc*. **1968**, *90*, 4064−4069.